



Geophysical Research Letters

RESEARCH LETTER

10.1002/2017GL073720

Key Points:

- InSAR supported by CGPS measurements confirm precursory inflation prior to the 2015 eruptions at Cotopaxi volcano
- Deformation is attributed to an opening sheet intrusion beneath the SW flank that contributed to internal edifice growth
- Preexisting structures may guide ascending magma under the volcano's SW flank, explaining the noncentrality of the observed deformation

Supporting Information:

- Supporting Information S1

Correspondence to:

A. M. Morales Rivera,
amorales@rsmas.miami.edu

Citation:

Morales Rivera, A. M., F. Amelung, P. Mothes, S.-H. Hong, J.-M. Nocquet, and P. Jarrin (2017), Ground deformation before the 2015 eruptions of Cotopaxi volcano detected by InSAR, *Geophys. Res. Lett.*, 44, doi:10.1002/2017GL073720.

Received 14 FEB 2017

Accepted 8 JUN 2017

Accepted article online 9 JUN 2017

Ground deformation before the 2015 eruptions of Cotopaxi volcano detected by InSAR

Anieri M. Morales Rivera¹ , Falk Amelung¹ , Patricia Mothes² , Sang-Hoon Hong³ , Jean-Mathieu Nocquet⁴ , and Paul Jarrin²

¹Rosenstiel School of Marine and Atmospheric Science, University of Miami, Miami, Florida, USA, ²Instituto Geofísico, Escuela Politécnica Nacional, Quito, Ecuador, ³Department of Geological Sciences, Pusan National University, Pusan, South Korea, ⁴Geoazur, IRD, Observatoire de la Côte d'Azur, CNRS, Université Côte d'Azur, Valbonne, France

Abstract Cotopaxi volcano started a period of volcanic unrest in April 2015 that led to a series of eruptions between August and November 2015. We use COSMO-SkyMed Interferometric Synthetic Aperture Radar supported by continuous GPS observations spanning the period of 2014–2016 to obtain time-dependent ground deformation data over Cotopaxi volcano related to the period of unrest and onset of eruptions. We find evidence of precursory deformation, with a maximum uplift on the western flank of 3.4 cm from April to August 2015. Deformation is explained by an inclined sheet intrusion located a few km southwest of the summit with an opening volume of $6.8 \times 10^6 \text{ m}^3$, extending from a depth of 12.1 km and shallowing to 5.5 km below the summit, that contributed to internal edifice growth. The temporal coincidence of deformation prior to the eruptions potentially suggests that short-term eruptions at Cotopaxi are partly controlled by episodic edifice growth.

1. Introduction

Volcanic eruptions are inevitably preceded by the ascent of new magma toward shallow levels and are often accompanied by surface deformation [Biggs *et al.*, 2014], offering the opportunity for early hazard identification using geodetic observations [e.g., Biggs and Pritchard, 2017; Dzurisin, 2006; Sparks, 2003]. Although pre-eruptive inflation has proven to be an invaluable source for volcanic hazard assessment, there are many examples of stratovolcano eruptions without observed inflation [e.g., Ebmeier *et al.*, 2013; Lu and Dzurisin, 2014; Morales Rivera *et al.*, 2016]. This can be explained by (1) either there was no inflation or (2) it was not resolved by the available geodetic data due to limited temporal and spatial resolution.

The 2015 eruptions at Cotopaxi stratovolcano in Ecuador were covered by the COSMO-SkyMed satellite constellation, providing the opportunity to increase deformation observations using satellite constellations with shorter revisit period. We use Interferometric Synthetic Aperture Radar (InSAR) time series supported by continuous GPS (CGPS) to investigate the volcanic processes during and after the 2015 unrest and eruptive periods at Cotopaxi. We furthermore highlight the key advantage of using satellite constellations to detect short-term pre-eruptive deformation signals of small amplitude on stratovolcanoes, which are more commonly observed as long-term signals [e.g., Chaussard and Amelung, 2012; Henderson and Pritchard, 2013].

1.1. Geological Framework

Cotopaxi stands on the margin between the NNE-SSW elongated Interandean valley depression and the Eastern Cordillera (a region with a compressive stress regime). The Interandean valley mainly consists of unconsolidated Quaternary volcanic deposits and material that has been eroded from the surrounding ridges, while the Eastern Cordillera is a Paleozoic to Cretaceous metamorphic belt [Hall and Calle, 1982]. This produces differences in the mechanical properties of the rocks in the Western and Eastern flanks of the volcano, potentially making the eastern side more resistant to deformation.

Cotopaxi is located within a shear zone derived from differential crustal shortening rates north and south of the volcano, resulting in a transcurrent to transpressive setting [Alvarado *et al.*, 2016; Fiorini and Tibaldi, 2012]. Magmatic emplacement is likely favored along main tectonic lineaments but poorly understood at Cotopaxi due to the limited exposure of structural features that are covered by Quaternary deposits [Fiorini and Tibaldi, 2012].

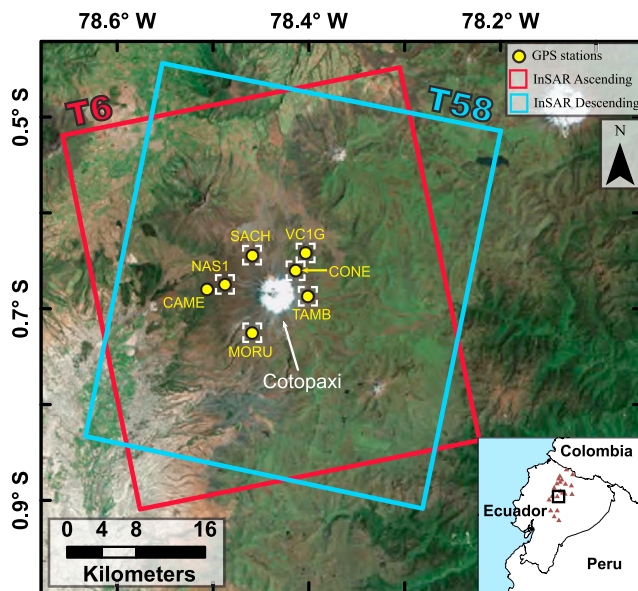


Figure 1. Cotopaxi volcano and surroundings, showing the location of data set features. Red square: InSAR ascending track 6 frame extent. Blue square: InSAR descending track 58 frame extent. Yellow circles: location of CGPS stations operated by IGEPN. White corner markers: area used to obtain InSAR average displacement time series plots shown in Figures 3 and S11. Inset: Brown triangles are active volcanoes during the Holocene [Siebert et al., 2010]; Black box is the figure extent over Cotopaxi and surroundings. Satellite image source: Esri ArcGIS® world imagery basemap.

new eruptive phase was preceded by increasing number of seismic events and SO_2 fluxes since mid-April and the end of May of 2015, respectively [Bernard et al., 2016; Gaunt et al., 2016; Instituto Geofisico, Escuela Politecnica Nacional (IGEPN), 2016].

2. InSAR and GPS Data

2.1. InSAR

Our data set (Table S1 in the Supporting Information) consists of 33 SAR scenes from ascending track 6 and 36 SAR scenes from descending track 58 acquired between August of 2014 and April of 2016 by the COSMO-SkyMed (CSK) satellite constellation of the Italian Space Agency, which has a revisit time of 1, 3, 4, 8, and 16 days (our data have mostly 16 day repeat pass). We inverted the generated network of interferograms to obtain the line-of-sight (LOS) displacement history and averaged LOS velocities. Further details on the InSAR data set, processing approach, and quality assessment of the displacement time series are found in the supporting information (Text S1).

2.2. GPS

Instituto Geofisico, Escuela Politecnica Nacional (IGEPN) had seven CGPS stations (Figure 1) within Cotopaxi edifice operating during the 2014–2016 analysis period [Mothes et al., 2013], but only six of these (SACH, VC1G, CONE, TAMB, MORU, and NAS1) were within the zone with coherent InSAR data and used for support of the InSAR measurements. Further details on the GPS data set and processing approach are found in the supporting information (Text S1).

3. Characteristics of Crustal Deformation From 2014 to 2016

Based on the seismic and eruptive activity (discussed below) we consider three time periods to characterize the changes in surface displacement at Cotopaxi: the pre-unrest period, the pre-eruptive unrest (including one InSAR epoch after the first eruption because of too few epochs), and the eruptive/post-eruptive period. We refer to them as periods 1, 2, and 3, respectively. Figure 2 shows the spatial patterns of InSAR LOS

1.2. Cotopaxi Volcano

Cotopaxi (5897 m, Figure 1) is an active glaciated Quaternary stratovolcano in a tectonically complex area of central Ecuador with a history of explosive eruptions that have resulted in the generation of massive lahars that have traveled over 300 km [Mothes, 1992; Mothes et al., 1998], making eruptions at this volcano a threat to infrastructure and over 250,000 people living along main rivers borne on Cotopaxi's flanks, south of the Ecuadorian capital, Quito [Aguilera et al., 2004].

After nearly 73 years of eruptive quiescence [Barberi et al., 1995], Cotopaxi had a series of phreatomagmatic to magmatic eruptions that started on 14 August of 2015 and continued until 30 November of the same year [Gaunt et al., 2016], erupting a total ash volume of $8.6 \times 10^5 \text{ m}^3$ and assigned a Volcanic Explosivity Index of 2 [Bernard et al., 2016]. The start of the

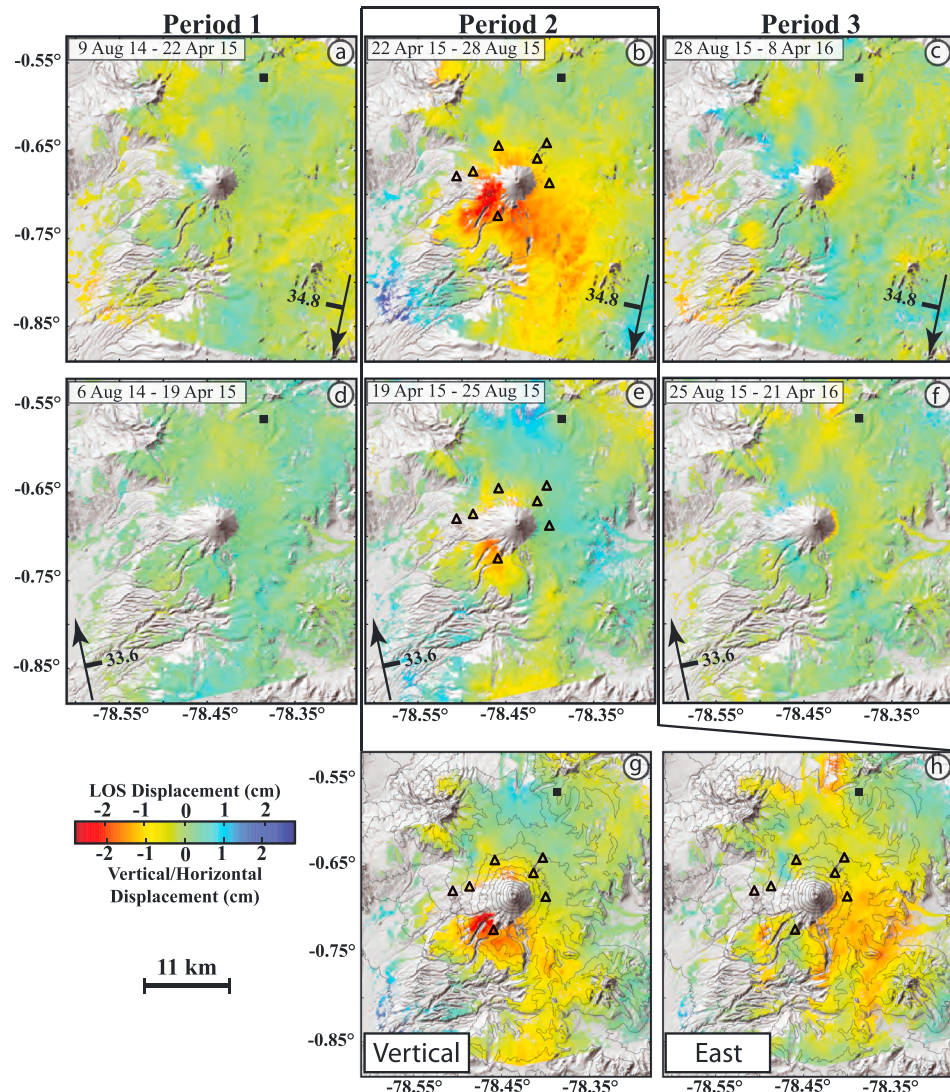


Figure 2. InSAR time series LOS displacement maps for COSMO-SkyMed (a–c) descending and (d–f) ascending satellite orbits. LOS displacement from August 2014 to April 2015 (Figures 2a and 2d). LOS displacement from April to August 2015 (Figures 2b and 2e). LOS displacement from August 2015 to April 2016 (Figures 2c and 2f). Observed deformation during period 2 (Figures 2b and 2e), decomposed into (g) vertical and (h) east displacement components. Arrows: the satellite flight direction. Black bars and numbers perpendicular to the arrows: satellite look direction with average radar look angle. Black triangles: CPGS stations. Black square: reference pixel.

displacement for both ascending and descending satellite orbits during these periods. Positive LOS displacements (LOS decrease, red colors) represent movement toward the satellite (e.g., uplift), and negative LOS displacements (LOS increase, blue colors) represent movement away from the satellite (e.g., subsidence). The top of the volcano is decorrelated due to the presence of a permanent glacier. Coherence is also lost over the western flank of the volcano mainly due to the 2015 eruptive deposits.

Our results do not show evident deformation during periods 1 and 3 (Figures 2a, 2d, and 2c, 2f) but reveal subtle deformation during period 2 (Figures 2b and 2e), correlating with the period of increased long period and tremor events (since April and June, respectively) prior to the 2015 eruptions (see Figure 3b). The strongest signal appears in both ascending and descending tracks in the SW flank of the volcano, indicating a dominant vertical displacement in that region. The descending data also show a large ellipsoidal pattern in the southern flank (Figure 2b) with a NW-SE major axis that is not evident in the ascending data (Figure 2e). We decomposed the observed deformation from the ascending and descending geometries into east-west and vertical

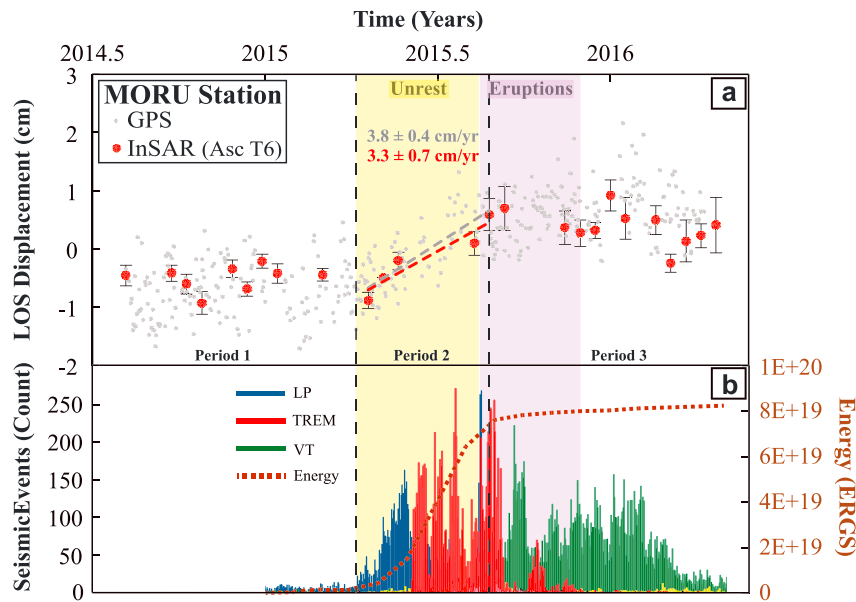


Figure 3. (a) Colocated InSAR (red circles; ascending T6) and GPS (gray dots; displacements projected into ascending T6 LOS) displacement time series at MORU station. InSAR error bars: standard deviation for all the coherent points within the area over MORU station (delimited by the white corner markers in Figure 1) at each epoch. Colored area: phases of pre-eruptive (yellow) and eruptive (purple) activity. Vertical dashed black lines: separation between periods identified in Figure 2. Inclined dashed lines: best-fitting linear regression during period 2 for InSAR (red) and GPS (gray) data with the corresponding deformation rate and standard error. (b) Seismic events and related energy released within the Cotopaxi edifice [Bernard et al., 2016; Gaunt et al., 2016]. Vertical solid lines: blue, red, and green are respectively long period (LP), tremor (TREM), and volcano-tectonic (VT) events. Dashed red line: Cumulative energy released by seismic events.

components (the north-south component was considered negligible due to near polar orbits of the satellites) [e.g., Wright et al., 2004] and found that this discrepancy can be explained by the differences in satellite viewing geometries (see Figure 2). The mean displacements and associated standard deviations outside of the suspected deforming region during period 2 provide estimates of the background noise, of $0.12 \pm 0.44 \text{ cm}$ and $0.32 \pm 0.45 \text{ cm}$ for vertical and east components, respectively. The peak motion is in the vertical component with a maximum uplift of 3.4 cm in the SW flank (-0.6993 and -78.4688), ~3 km NW of MORU station.

Figure 3a shows the average InSAR LOS displacements and standard deviations for an area centered over MORU GPS station (see Figure 1 for extents) compared to the GPS displacements projected into the COSMO-SkyMed satellite's LOS directions. For the complete GPS and InSAR time series see Figures S10 and S11. The LOS trends observed with InSAR and GPS generally agree and are consistent with an inflating source at depth during period 2 (Text S2 and Table S6). The time series also shows that the edifice remained inflated during and after the eruptions, as evidenced by the lack of any displacement signal during period 3.

4. Source Models for the Volcanic Deformation

We model the observed deformation using the best-fitting solutions for magmatic sources embedded in a homogeneous and isotropic elastic half-space. Point sources [Mogi, 1958] and penny-shaped cracks [Fialko et al., 2001] produce circular vertical deformation patterns, inconsistent with the observed elongated and asymmetrical pattern (Figure 2g). We therefore use a rectangular dislocation with uniform opening [Okada, 1985]. The data are InSAR LOS velocities from both ascending and descending orbits, sampled using uniform grids to reduce the amount of data points (each grid dimension was nearly $400 \times 400 \text{ m}$). The InSAR data were weighted equally. The GPS data are excluded from the main modeling but are jointly inverted with InSAR data in the supporting information (1) due to limited coverage over the region with highest displacement (MORU being the only station in the southern flank), (2) because the magnitude of the GPS-derived horizontal velocities (Table S5) were generally below the InSAR noise level (see section 3 for explanation on

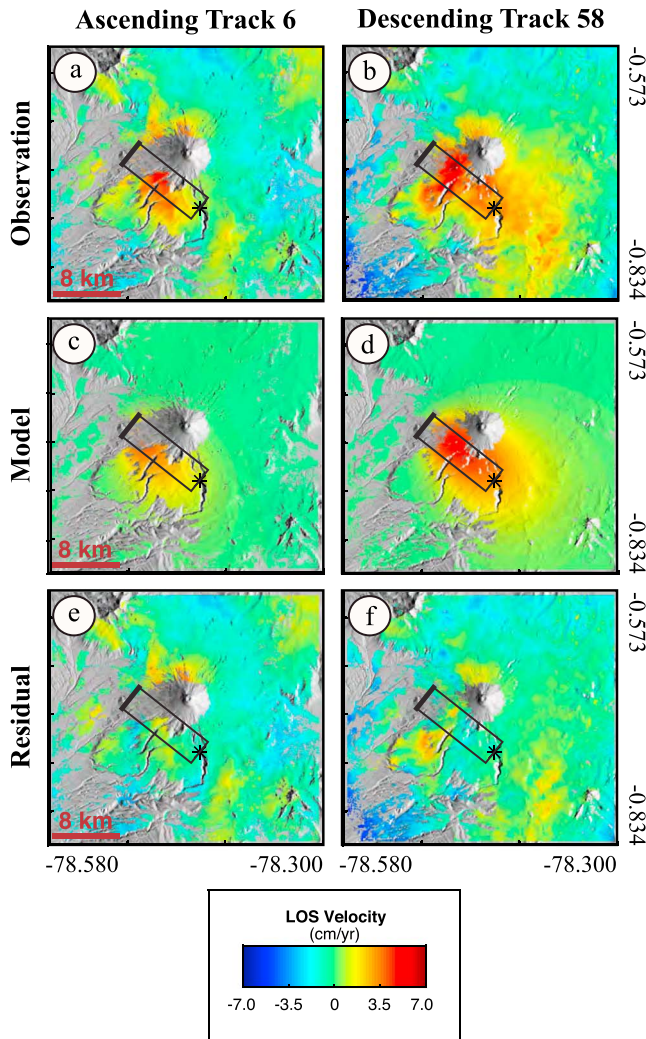


Figure 4. (a, b) Average LOS velocity during period 2. (c, d) Predicted average LOS velocity from the best-fitting models for the same period. (e, f) Difference between the observed and predicted LOS velocity (residuals). The black rectangles outline the geometry of the best-fitting planar source (sheet intrusion), the thicker line representing the shallower edge, and the asterisk representing the downdip depth.

(that both exclude and account for a possible translation error in the GPS-derived deformation) furthermore show a best-fitting sheet intrusion beneath the SW flank of the volcano (Text S3 and S4 of the supporting information).

5. Discussion

We have observed precursory inflation of the southwestern flank of the volcano, starting with the onset of long period seismic events in April 2015, which we explained by an opening sheet intrusion that initiated at 6.2 km depth below sea level and reached to just above sea level. This model for the magmatic source is highly simplified because the signal amplitude is small (<3 cm LOS) and because we have neglected the hot and mechanically heterogeneous crustal conditions near a magmatic source, possible interactions with crustal faults, and the geological differences east and west of Cotopaxi (as mentioned in section 1.1), but provides a first-order estimate for source depth, geometry, and volume change.

An intrusion into this part of the volcano (see Figure 4) is consistent with an inflating source during the 2001–2002 unrest identified using sparse electronic distance meter measurements [Hickey et al., 2015]. Both

negligible northing component and easting component background noise levels in InSAR measurements), and (3) due to a possible translation error in the GPS-derived deformation (see Text S3). We solve the geophysical inverse problems using a Monte Carlo-based Gibbs sampling algorithm [Brooks and Frazer, 2005] to find the optimal solutions that yield the lowest root-mean-square error (RMS).

From the modeled geometries, we find an opening dislocation located beneath the southwest flank of the volcano to be the best fit to our InSAR observations (Figure 4 and Table S7). The intrusion is 11.9 km long, 3.0 km wide, upward dipping toward the northwest at 33° with an opening of 0.2 m, corresponding to a volume of $6.8 \times 10^6 \text{ m}^3$, probably representing an inclined sheet intrusion. The source depth was located 7 km SSE of the volcano's summit at a depth of 12.1 km below the summit (6.2 km below sea level (bsl)), with the shallowest portion extending to 5.5 km below the summit (0.4 km above sea level). The modeled parameters with their trade-offs and confidence intervals are reported in the supporting information (Figure S12 and Table S7). We also tested a pressurized ellipsoid source [Yang et al., 1988] but found a poorer fit (Table S8). The model-predicted horizontal velocities provide a poor fit to the CGPS data (Figure S13), but joint InSAR and GPS inversions

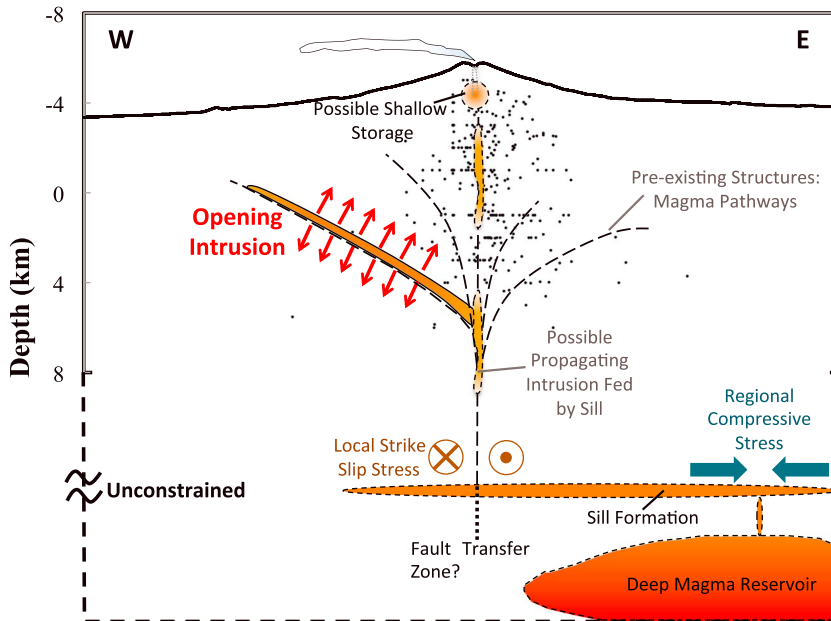


Figure 5. Interpretative schematic illustrating the effects of local and regional tectonics on magma storage and ascent at Cotopaxi volcano. Dashed lines: unconstrained features. Black dots: seismic events (long period, tremor, volcano-tectonic, and hybrid events) during the 2015 period of deformation (provided by IGEPN).

intrusions coincided with the timing of increased seismicity but were not spatially associated with the latter (see earthquake locations in Figures 5 and S19), what Hickey *et al.* [2015] attributed for the 2001–2002 intrusion to a zone of ductility because the rocks were heated and weakened by the presence of magma. Aseismic intrusions have also been suggested to occur due to dilation of pathways from increasing volatile pressure without breaking the rock [Poland *et al.*, 2014], aseismic strain accommodation due to local stress conditions [Calais *et al.*, 2008], magma accumulation near the brittle-ductile transition, or episodic intrusions that heat the crust sufficiently to maintain a ductile zone [Lu *et al.*, 2002].

5.1. Internal Edifice Growth by Episodic Intrusion

The notion that the geodetically inferred aseismic intrusion did neither propagate toward the summit crater nor erupted is further supported by the observation about the edifice remaining inflated during and after the eruptions, suggesting that the bulk of the intruded magma either remains beneath the edifice in a liquid or mushy phase or has solidified. This could be related to an episode of internal (endogenous) edifice growth induced by the intrusion, which has been directly observed at basaltic volcanoes [e.g., Francis *et al.*, 1993] and during silicic dome formation [e.g., Kaneko *et al.*, 2002; Swanson *et al.*, 1987], but not commonly at stratovolcanoes (edifice wide). One of the observed examples of stratovolcano growth was within the Ecuadorian Eastern Cordillera at Tungurahua volcano [Biggs *et al.*, 2010], suggesting that it could be a common process within volcanoes of this Cordillera and could be potentially observed more frequently from short-term deformation signals at stratovolcanoes worldwide through improved temporal geodetic sampling.

Our observations are unique because not only do we record one of the few cases of directly observed internal edifice growth of a stratovolcano from an episodic intrusion, but because it preceded an eruption it suggests that short-term eruptive behavior could be partly controlled by episodes of edifice growth. This has been suggested for long-term eruptive behavior [Pinei *et al.*, 2010] but is often ignored for short-term eruptions due to their complex and irregular nature. Internal growth may induce stress variations and the likelihood of magmatic gas accumulation within the system [e.g., Kaneko *et al.*, 2002], which can ultimately result in explosive eruptions such as those observed at Cotopaxi.

5.2. Secondary Propagating Intrusion

Most of the seismic events during the period of unrest (dominantly long period and spasmodic tremor events) occurred vertically beneath the edifice (see Figure 5), suggesting vertical fluid migration (gas or

magma) through preexisting structures and/or conduits [Molina *et al.*, 2008] from a magma body at depth. We therefore suggest that a secondary intrusion of magma propagated toward the summit. This intrusion is further supported by the occurrence of volcano-tectonic events beneath the edifice during the eruption phase [Gaunt *et al.*, 2016], which suggests the fracturing of rock by migration of magma. The initiation depth of the modeled inclined sheet (6.2 km bsl) also corresponds to the base of the region of seismic events (see Figure 5), further supporting migration of magma from a deeper source.

We note that we lack of geodetic evidence to support the presence of a deep reservoir (below 6.2 km bsl) beneath Cotopaxi because no deformation of such a source was detected. Moreover, our data do not constrain if newly intruded magma from a deeper source actually erupted. Fluid migration toward the summit from deeper sources (as suggested by seismicity) coinciding with internal edifice growth (as suggested by deformation) could have put shallower storage zones in a critical state, promoting failure and eruption. Furthermore, the $<1 \text{ Mm}^3$ of erupted magma was shown to be from a shallow source based upon the high percentage of erupted microlites that are interpreted to be from magma crystallization at shallow depths [Gaunt *et al.*, 2016].

The geodetic data do not exclude the possibility of a shallow vertically propagated intrusion or storage region because there is no data for the volcano's $\sim 14 \text{ km}^2$ [Pistolesi *et al.*, 2014] summit glacier due to phase decorrelation. Other possible reasons for the lack of detected deformation of a shallower source are discussed by Morales Rivera *et al.* [2016]. The relatively poor fit of the modeled deformation to the horizontal GPS with a central, roughly radial pattern (Figure S13) could indicate the presence of a shallow source, but we lack sufficient data to properly constrain it (see Text S3 for further discussion).

5.3. Conceptual Model of Magma Storage and Ascent

Our observations together with the regional and local tectonics lead to a new conceptual model for magma ascent and storage at Cotopaxi volcano (Figure 5). In the regional compressive stress regime of the Northern Andes, magma ascends from deeper reservoirs and is typically emplaced in form of horizontal sills [e.g., Chaussard and Amelung, 2014; Gudmundsson, 2012]. Cotopaxi, however, is located in a fault transfer zone in which the horizontal greatest and least principal stresses [Fiorini and Tibaldi, 2012] favor the vertical propagation of magma along zones of weakness such as interfaces between geologic units, faults, and fractures [Mathieu and Vries, 2009]. From a depth deeper than 6.2 km bsl, some intrusions will propagate toward shallower levels and later erupt at the summit, while others, such as our modeled intrusion, will remain within the subsurface without erupting, the latter occasionally contributing to internal edifice growth which could potentially induce stress changes within the shallow volcanic system. Shallow storage zones are common in strike-slip stress regimes [e.g., Chaussard and Amelung, 2012], and although it was not constrained with geodetic data, it was suggested to be the source of the 2015 eruptive products [Gaunt *et al.*, 2016]. The SO₂ emissions before and during the eruptive period [IGEPN, 2016] also require the presence of either an ascending magma or a shallow magma storage at a depth where SO₂ exsolves from the magma (typically $<5 \text{ km}$ below the summit) [e.g., López *et al.*, 2013; Sutton and Elias, 2014].

6. Summary and Conclusions

The InSAR data have revealed $\leq 3.4 \text{ cm}$ of uplift of Cotopaxi's SW flank ~ 4 months prior to the start of the most recent eruption phase, consistent with GPS data. Such small amplitude deformation signals at stratovolcanoes are more commonly observed in InSAR analyses as long-term signals. Thus, we highlight the advantage of using satellite systems with short revisit periods to monitor short-term, small amplitude deformation signals.

We attribute the observed deformation to the inflation of an inclined sheet intrusion that stalled beneath the edifice under the SW flank and contributed to internal edifice growth. The temporal coincidence of deformation and seismicity prior to the eruption suggests that short-term eruptive behavior at Cotopaxi could be partly controlled by processes induced by internal edifice growth from episodic intrusions. Future studies that focus on modeling stress distributions resulting from episodic internal edifice growth, incorporating detailed topographic and subsurface properties, could be beneficial to gain more insights about short-term pre-eruptive processes at stratovolcanoes worldwide and valuable for eruption forecasting.

We did not detect any surface deformation related to inflation or deflation of a shallow or deeper magma chamber, possibly due to small volumes of intruded magma (as suggested by the volumes of the modeled intrusion and erupted material). Preexisting structures may guide ascending magma under the SW flank of the volcano, explaining the noncentrality of the observed ground deformation that resulted in internal edifice growth.

Acknowledgments

COSMO-SkyMed data were provided by the Italian Space Agency (ASI) through the Group on Earth Observation's Geohazard Supersite initiative [Amelung et al., 2015] and made available by the UNAVCO Facility's SAR data sharing system, supported by the National Science Foundation (NSF) and National Aeronautics and Space Administration (NASA) under NSF Cooperative Agreement EAR-0735156. InSAR time series analysis and postprocessing was conducted using the PySAR software, developed by Heresh Fattah and Yunjun Zhang (<https://github.com/yunjunz/PySAR>). The University of Miami's GeodMod software was used for the modeling. InSAR data products can be obtained at <http://insarmaps.miami.edu/>. We thank the staff at IGEPN for instrument maintenance, data processing, and monitoring the unrest and eruption of Cotopaxi volcano and the NASA Earth Science Division for funding (NNX14AL39G). We also thank Francisco Delgado, Michael Lisowski, and Andrew Newman for their detailed and constructive suggestions that contributed to improvements in our paper.

References

- Aguilera, E., M. T. Pareschi, M. Rosi, and G. Zanchetta (2004), Risk from lahars in the Northern Valleys of Cotopaxi Volcano (Ecuador), *Nat. Hazards*, 33(2), 161–189, doi:10.1023/b:nahaz.0000037037.03155.23.
- Alvarado, A., L. Audin, J. M. Nocquet, E. Jaillard, P. Mothes, P. Jarrín, M. Segovia, F. Rolandone, and D. Cisneros (2016), Partitioning of oblique convergence in the Northern Andes subduction zone: Migration history and the present-day boundary of the North Andean Sliver in Ecuador, *Tectonics*, 35, 1048–1065, doi:10.1002/2016TC004117.
- Amelung, F., E. J. Fielding, and S. Sigmundsson (2015), EO for the mitigation of geological disasters, Rep., pp. 50–53. [Available at http://www.eohandbook.com/eohb2015/case_study_8.html.]
- Barberi, F., M. Coltellini, A. Frullani, M. Rosi, and E. Almeida (1995), Chronology and dispersal characteristics of recently (last 5000 years) erupted tephra of Cotopaxi (Ecuador): Implications for long-term eruptive forecasting, *J. Volcanol. Geotherm. Res.*, 69(3–4), 217–239, doi:10.1016/0377-0273(95)00017-8.
- Bernard, B., J. Battaglia, A. Proaño, S. Hidalgo, F. Vásconez, S. Hernandez, and M. Ruiz (2016), Relationship between volcanic ash fallouts and seismic tremor: Quantitative assessment of the 2015 eruptive period at Cotopaxi volcano, Ecuador, *Bull. Volcanol.*, 78(11), 80, doi:10.1007/s00445-016-1077-5.
- Biggs, J., and M. E. Pritchard (2017), Global volcano monitoring: What does it mean when volcanoes deform?, *Elements*, 13(1), 17–22, doi:10.2113/gselements.13.1.17.
- Biggs, J., P. Mothes, M. Ruiz, F. Amelung, T. H. Dixon, S. Baker, and S. H. Hong (2010), Stratovolcano growth by co-eruptive intrusion: The 2008 eruption of Tungurahua Ecuador, *Geophys. Res. Lett.*, 37, L21302, doi:10.1029/2010GL044942.
- Biggs, J., S. K. Ebmeier, W. P. Aspinall, Z. Lu, M. E. Pritchard, R. S. J. Sparks, and T. A. Mather (2014), Global link between deformation and volcanic eruption quantified by satellite imagery, *Nat. Commun.*, 5, doi:10.1038/ncomms4471.
- Brooks, B. A., and L. N. Frazer (2005), Importance reweighting reduces dependence on temperature in Gibbs samplers: An application to the coseismic geodetic inverse problem, *Geophys. J. Int.*, 167(1), 12–20, doi:10.1111/j.1365-246X.2005.02573.x.
- Calais, E., et al. (2008), Strain accommodation by slow slip and dyking in a youthful continental rift, East Africa, *Nature*, 456(7223), 783–787.
- Chaussard, E., and F. Amelung (2012), Precursory inflation of shallow magma reservoirs at west Sunda volcanoes detected by InSAR, *Geophys. Res. Lett.*, 39, L21311, doi:10.1029/2012GL053817.
- Chaussard, E., and F. Amelung (2014), Regional controls on magma ascent and storage in volcanic arcs, *Geochem., Geophys., Geosyst.*, 15, 1407–1418, doi:10.1002/2013GC005216.
- Dzurisin, D. (2006), *Volcano Deformation: Geodetic Monitoring Techniques*, pp. 223–278, Springer, Berlin.
- Ebmeier, S. K., J. Biggs, T. A. Mather, and F. Amelung (2013), On the lack of InSAR observations of magmatic deformation at Central American volcanoes, *J. Geophys. Res. Solid Earth*, 118, 2571–2585, doi:10.1002/jgrb.50195.
- Fialko, Y., Y. Khazan, and M. Simons (2001), Deformation due to a pressurized horizontal circular crack in an elastic half-space, with applications to volcano geodesy, *Geophys. J. Int.*, 146(1), 181–190, doi:10.1046/j.1365-246X.2001.00452.x.
- Florini, E., and A. Tibaldi (2012), Quaternary tectonics in the central Interandean Valley, Ecuador: Fault-propagation folds, transfer faults and the Cotopaxi Volcano, *Global Planet. Change*, 90–91, 87–103, doi:10.1016/j.gloplacha.2011.06.002.
- Francis, P., C. Oppenheimer, and D. Stevenson (1993), Endogenous growth of persistently active volcanoes, *Nature*, 366(6455), 554–557.
- Gaunt, H. E., B. Bernard, S. Hidalgo, A. Proaño, H. Wright, P. Mothes, E. Criollo, and U. Kueppers (2016), Juvenile magma recognition and eruptive dynamics inferred from the analysis of ash time series: The 2015 reawakening of Cotopaxi volcano, *J. Volcanol. Geotherm. Res.*, 328, 134–146, doi:10.1016/j.jvolgeores.2016.10.013.
- Gudmundsson, A. (2012), Magma chambers: Formation, local stresses, excess pressures, and compartments, *J. Volcanol. Geotherm. Res.*, 237–238, 19–41, doi:10.1016/j.jvolgeores.2012.05.015.
- Hall, M. L., and J. Calle (1982), Geochronological control for the main tectonic-magmatic events of Ecuador, *Earth Sci. Rev.*, 18(3), 215–239, doi:10.1016/0012-8252(82)90038-1.
- Henderson, S. T., and M. E. Pritchard (2013), Decadal volcanic deformation in the Central Andes Volcanic Zone revealed by InSAR time series, *Geochem., Geophys., Geosyst.*, 14, 1358–1374, doi:10.1002/ggpe.20074.
- Hickey, J., J. Gottsmann, and P. Mothes (2015), Estimating volcanic deformation source parameters with a finite element inversion: The 2001–2002 unrest at Cotopaxi Volcano, Ecuador, *J. Geophys. Res. Solid Earth*, 120, 1473–1486, doi:10.1002/2014JB011731.
- Instituto Geofísico, Escuela Politécnica Nacional (IGEPN) (2016), Actualización de la Actividad Eruptiva del Volcán Cotopaxi—Nº5, Rep., Instituto Geofísico, Escuela Politécnica Nacional. [Available at <http://www.igepn.edu.ec/cotopaxi/informes-cotopaxi/coto-especiales/coto-e-2016/14621-informe-especial-cotopaxi-n-05/file/>.]
- Kaneko, T., M. J. Wooster, and S. Nakada (2002), Exogenous and endogenous growth of the Unzen lava dome examined by satellite infrared image analysis, *J. Volcanol. Geotherm. Res.*, 116(1–2), 151–160, doi:10.1016/S0377-0273(02)00216-0.
- López, T., S. Ushakov, P. Izbekov, F. Tassi, C. Cahill, O. Neill, and C. Werner (2013), Constraints on magma processes, subsurface conditions, and total volatile flux at Bezymianny Volcano in 2007–2010 from direct and remote volcanic gas measurements, *J. Volcanol. Geotherm. Res.*, 263, 92–107, doi:10.1016/j.jvolgeores.2012.10.015.
- Lu, Z., and D. Dzurisin (2014), *InSAR Imaging of Aleutian Volcanoes: Monitoring a Volcanic Arc from Space*, 1 edn., pp. 347–364, Springer, Berlin Heidelberg, doi:10.1007/978-3-642-00348-6.
- Lu, Z., C. Wicks, D. Dzurisin, J. A. Power, S. C. Moran, and W. Thatcher (2002), Magmatic inflation at a dormant stratovolcano: 1996–1998 activity at Mount Peulik volcano, Alaska, revealed by satellite radar interferometry, *J. Geophys. Res.*, 107(B7), 2134, doi:10.1029/2001JB000471.
- Mathieu, L., and B. V. W. D. Vries (2009), Edifice and substrata deformation induced by intrusive complexes and gravitational loading in the Mull Volcano (Scotland), *Bull. Volcanol.*, 71(10), 1133, doi:10.1007/s00445-009-0295-5.
- Mogi, K. (1958), Relations between the eruptions of various volcanoes and the deformations of the ground surfaces around them, *Bull. Earthq. Res. Inst., Univ. Tokyo*, 36, 99–134.

- Molina, I., H. Kumagai, A. García-Aristizábal, M. Nakano, and P. Mothes (2008), Source process of very-long-period events accompanying long-period signals at Cotopaxi Volcano, Ecuador, *J. Volcanol. Geotherm. Res.*, 176(1), 119–133, doi:10.1016/j.jvolgeores.2007.07.019.
- Morales Rivera, A. M., F. Amelung, and P. Mothes (2016), Volcano deformation survey over the Northern and Central Andes with ALOS InSAR time series, *Geochem., Geophys., Geosyst.*, 17, 2869–2883, doi:10.1002/2016GC006393.
- Mothes, P. A. (1992), Lahars of Cotopaxi Volcano, Ecuador: Hazard and risk evaluation, in *Geohazards: Natural and man-made*, edited by G. J. H. McCall, D. J. C. Laming and S. C. Scott, pp. 53–63, Springer, Dordrecht, Netherlands, doi:10.1007/978-94-011-2310-5_7.
- Mothes, P. A., M. L. Hall, and R. J. Janda (1998), The enormous Chillos Valley lahar: An ash-flow-generated debris flow from Cotopaxi Volcano, Ecuador, *Bull. Volcanol.*, 59(4), 233–244, doi:10.1007/s004450050188.
- Mothes, P. A., J.-M. Nocquet, and P. Jarrín (2013), Continuous GPS network operating throughout Ecuador, *Eos. Trans. AGU*, 94(26), 229–231, doi:10.1002/2013EO260002.
- Okada, Y. (1985), Surface deformation due to shear and tensile faults in a half-space, *Bull. Seismol. Soc. Am.*, 75(4), 1135–1154.
- Pinel, V., C. Jaupart, and F. Albino (2010), On the relationship between cycles of eruptive activity and growth of a volcanic edifice, *J. Volcanol. Geotherm. Res.*, 194(4), 150–164, doi:10.1016/j.jvolgeores.2010.05.006.
- Pistolesi, M., R. Cioni, M. Rosi, and E. Aguilera (2014), Lahar hazard assessment in the southern drainage system of Cotopaxi Volcano, Ecuador: Results from multiscale lahar simulations, *Geomorphology*, 207, 51–63, doi:10.1016/j.geomorph.2013.10.026.
- Poland, M. P., A. Miklius, and E. K. Montgomery-Brown (2014), Chapter 5: Magma supply, storage, and transport at shield-stage Hawaiian volcanoes, US Geol. Surv. Professional Pap. 1801, Characteristics of Hawaiian Volcanoes.
- Siebert, L., T. Simkin, and P. Kimberly (2010), *Volcanoes of the World*, 3rd ed., 568 pp., Univ. of Calif. Press, Berkeley.
- Sparks, R. S. J. (2003), Forecasting volcanic eruptions, *Earth Planet. Sci. Lett.*, 210(1–2), 1–15, doi:10.1016/S0012-821X(03)00124-9.
- Sutton, A. J., and T. Elias (2014), One hundred volatile years of volcanic gas studies at the Hawaiian Volcano Observatory, *Characteristics of Hawaiian Volcanoes*, US Geol. Surv. Prof. Pap., 1801, 295–320.
- Swanson, D. A., D. Dzurisin, R. T. Holcomb, E. Y. Iwatsubo, W. W. Chadwick, T. J. Casadevall, J. W. Ewert, and C. C. Heliker (1987), Growth of the lava dome at Mount St. Helens, Washington, (USA), 1981–1983, *Geol. Soc. Am. Spec. Pap.*, 212, 1–16, doi:10.1130/SPE212-p1.
- Wright, T. J., B. E. Parsons, and Z. Lu (2004), Toward mapping surface deformation in three dimensions using InSAR, *Geophys. Res. Lett.*, 31, L01607, doi:10.1029/2003GL018827.
- Yang, X.-M., P. M. Davis, and J. H. Dieterich (1988), Deformation from inflation of a dipping finite prolate spheroid in an elastic half-space as a model for volcanic stressing, *J. Geophys. Res.*, 93, 4249–4257, doi:10.1029/JB093iB05p04249.